EURASIP Journal on Wireless Communications and Networking

REVIEW Open Access

Survey on reconfigurable intelligent surfaces below 10 GHz

Visa Tapio[1*], Ibrahim Hemadeh[2], Alain Mourad[2], Arman Shojaeifard[2] and Markku Juntti[1]

*Correspondence: visa.tapio@oulu.fi
[1] Centre for Wireless Communications, University of Oulu, Oulu, Finland
Full list of author information is available at the end of the article

Abstract

Reconfigurable intelligent surface (RIS) is a programmable structure that can be used to control the propagation of electromagnetic waves by changing the electric and magnetic properties of the surface. By placing these surfaces in an environment, the properties of radio channels can be controlled. This opens up new opportunities to improve the performance of wireless systems. In this paper, the basic operation of antenna array and metasurface based RIS is described. While the current long term (6G) research on RIS often prioritizes very high frequencies from tens to hundreds of GHz, this paper puts emphasis rather on operating frequencies below 10 GHz which promise a much faster to market track for RIS applications. For this purpose, review of the literature on the use of RIS in wireless communication applications operating below 10 GHz frequency band is provided.

Keywords: Reconfigurable intelligent surface, Metasurface, 5G

1 Introduction

Reconfigurable intelligent surface (RIS)—known also as intelligent reflecting surface (IRS), and large intelligent surface (LIS)—is a programmable structure that can be used to control the propagation of electromagnetic (EM) waves by changing the electric and magnetic properties of the surface. In addition to the control of EM waves, RISs can be used to sense the radio environment by integrating sensing capabilities into them. By placing intelligent surfaces in the environment where wireless systems are operating, the properties of the radio channels can be controlled at least partially.

The control of radio channels changes the conventional wireless system design paradigm, in which the radio channel is seen as an uncontrollable entity that distorts the transmitted signals. Therein the transmitter (TX) and the receiver (RX) are designed to equalize the impact of the channel. Envisioned scenarios vary from cases where a single RIS is placed on a wall to direct signals coming from a predetermined direction, e.g., base station, to the environment where almost all surfaces (walls, furniture, clothes, etc.) are covered with a metasurface based RIS [1–4]. The introduction of intelligent surfaces can improve the reliability and energy efficiency of wireless systems. They may allow accurate localization of people and objects in environments where, for example, satellite-based positioning systems do not work properly [5, 6]. In radio equipment design,

intelligent surfaces realized with metasurfaces are anticipated to enable the realization of low-complexity and energy efficient transceivers that require only a limited, ideally one, active radio frequency (RF) chain [2, 3, 7].

Two approaches can be used to implement an RIS that control the impinging signals characteristics (e.g., reflection, refraction, absorption, focusing and polarization), namely, conventional antenna arrays and metasurfaces. In a nutshell, metasurfaces are electrically thin and dense two-dimensional arrays of structural elements possessing desired properties granted by their constitutive elements. Elements are called meta-cells, unit-cells or meta-atoms. The meta-cells size is much smaller than the signal's wavelength (λ) typically, between $\lambda/10$ and $\lambda/5$ [8, 9]. In addition to the control of EM propagation, metasurfaces can be used to realize complex operations such as data modulation and mathematical operations and they have been demonstrated to be capable of storing EM pulses for short time periods in the order of 15 ns [10, 11].

The RIS is mainly considered to be a beyond 5G technology operating at frequencies from tens of gigahertzs (GHz) to terahertzs (THz). At these frequency bands, the signal propagation is heavily attenuated and can be blocked completely by the obstacles in the propagation environment. Hence, the channels between a multi-antenna TX and RX are modeled as sparse channels and the direct link between the TX and RX is often assumed to be completely blocked. In these cases, the ability to form beams with moderate sized surfaces enables communication between the TX and RX.

2 Research method

This paper is a state-of-the art review on the application of the RIS below 10 GHz frequency. At these frequencies the channel between the TX and RX is not in general completely blocked by the obstacles and the channel is not modeled as a sparse channel. This means that the role of the RIS is not to enable the communication between the TX and RX as at higher frequencies, but to increase the capacity, although in some cases the coverage extension by directing the transmitted signal behind an obstacle such as a building in urban environment or a hill in sub-urban/rural environment is applicable also at sub-10 GHz frequencies. The purpose of this review is to explore the RIS implementation options for the existing 5G networks operating at the 5G NR Frequency Range 1 (FR1), but the survey is extended to frequencies up to 10 GHz.

3 Reflecting antenna arrays in RIS applications

3.1 Operation principle

Electrically tunable reflecting antenna arrays can be used to dynamically adjust their radiation patterns [12]. Hence, within the context of RIS, antenna arrays can be employed as reflecting structures. Specifically, a large number of low-cost and passive antenna elements are employed, which operate as reflectors with no need for RF chains as in the conventional multiple-input multiple-output (MIMO) systems using multiple transmit and multiple receive antennas. To expound, Fig. 1 describes the operation of an antenna array-based RIS, which relies on microstrip patch antennas. Note here that other antenna types can also be used as RIS reflectors.

The structure in Fig. 1 consists of a dielectric substrate with relative permittivity ϵ_r placed on a metallic ground plane. Metallic patch elements are placed on the

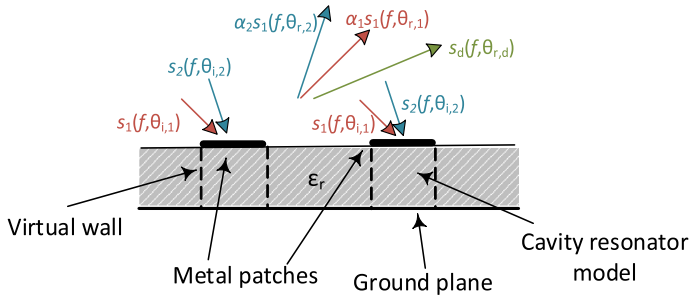

Fig. 1 Patch antenna array as a reflector

other side of the dielectric substrate. The inter-spacing distance between the metal patches in the array of Fig. 1 is typically in the order of $\lambda/2$ (λ= wavelength). A single patch antenna element can be modeled as a cavity resonator. Such a model consists of the patch, the dielectric directly below the patch, the ground plane as well as the virtual vertical walls (vertical dashed lines) shown in Fig. 1 [13]. When electromagnetic energy, with frequency equal to the resonance frequency of the cavity resonator, is coupled into the cavity, it starts to oscillate. This oscillating energy is then radiated by the antenna element, i.e., the incident signal is reflected. If the properties of all elements are the same, the reflection angle of the reflected waves is equivalent to the incident angle of impinging waves. This is illustrated in Fig. 1 where the incident signal $s_1(f,\theta_{i,1})$ coming from direction $\theta_{i,1}$ at frequency f is reflected to the specular direction $\theta_{r,1}$ as $\alpha_1 s_1(f,\theta_{r,1})$, where complex coefficient α_1 denotes the effect of the patch antenna. Similarly, the other incoming signal $s_2(f,\theta_{i,2})$ from direction $\theta_{i,2}$ is reflected towards $\theta_{r,2}$ as $\alpha_2 s_2(f,\theta_{r,2})$, which is different from the reflection direction of $s_1(f,\theta_{i,1})$. If the desired reflection angle is different from $\theta_{r,2}$, say $\theta_{r,d}$ in Fig. 1, then the phase responses of the individual elements should be changed so that $\alpha_2 s_2(f,\theta_{r,2}) = s_d(f,\theta_{r,d})$. This could be achieved by keeping the phase response of one element, say, the one on the left in Fig. 1, unchanged and tune the phase response of the other elements so that the aggregated waves reflecting on all the elements propagates towards the desired direction. The phase response of an antenna element changes, when its resonance frequency is changed. Hence, it can be controlled by connecting a varactor between the metallic patch and the ground plate [14]. By varying the bias voltage of the varactor, the reflection angle of the reflected wave can be steered electrically. More specifically, when the phase response of an element is changed, the reflection angles of all impinging waves are affected, such as the reflections of both $s_1(f,\theta_{i,1})$ and $s_2(f,\theta_{i,2})$ as can be seen in Fig. 1. This implies that the incident waves coming from different directions cannot, in general, be reflected into a common direction.

The model described above does not take into consideration the coupling effect between the neighboring elements, because the cavity resonator model cannot be used to model the coupling, but it provides a basic description of the reflection behavior in planar antenna arrays. To determine the phase shift required to steer the reflected EM wave toward a desired direction, consider the planar array model shown in Fig. 2. The black dots shown in the figure indicate the positions of the elements,

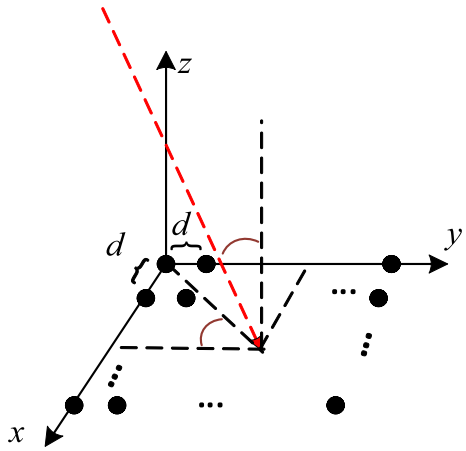

Fig. 2 Coordinate system for a reflect array

given that the element spacing d is equal over the x and y planes. When an EM wave impinges a planar array from the direction defined with the angle between the z-axis and the propagation direction of the wave (φ) and the propagation direction in $x-y$ plane (ϕ), the signal components on the $x-y$ plane are

$$\mathbf{X}_{\mathrm{RIS}}(x,y) = \mathbf{f}_1\mathbf{f}_2^T h_{\mathrm{BS}\to\mathrm{RIS}}(\varphi,\phi)x_{\mathrm{BS}}(\varphi,\phi) \tag{1}$$

where $x_{\mathrm{BS}}(\varphi,\phi)$ is the signal sent by a transmitter, e.g., base station (BS), and received by the planar array from (φ,ϕ) direction, $h_{\mathrm{BS}\to\mathrm{RIS}}(\varphi,\phi)$ is the channel between the base station and array seen by the signal x_{BS}, and vectors $\mathbf{f}_1$ and $\mathbf{f}_2$ are

$$\mathbf{f}_1 = [1\ e^{j\kappa d\sin u}\ e^{j\kappa 2d\sin u}\ \cdots\ e^{j\kappa(N-1)d\sin u}]^T \tag{2}$$

$$\mathbf{f}_2 = [1\ e^{j\kappa d\sin v}\ e^{j\kappa 2d\sin u}\ \cdots\ e^{j\kappa(N-1)d\sin v}]^T \tag{3}$$

where $\sin v = \sin\varphi\sin\phi$ and $\sin u = \sin\varphi\cos\phi$, and N and M are the numbers of elements in x and y directions, respectively. When (0,0,0) in Fig. 2 is selected as a reference point, the relative phase shift at point (n, m) on the planar array is

$$\psi(n,m) = \kappa(nd\sin\varphi\cos\phi + md\sin\varphi\sin\phi) \tag{4}$$

where $\kappa = 2\pi/\lambda$. In order to reflect the signal towards the (φ_r,ϕ_r) direction, the required relative phases of the elements are

$$\psi_r(n,m) = \kappa(nd\sin\varphi_r\cos\phi_r + md\sin\varphi_r\sin\phi_r) \tag{5}$$

This means that the phase of the element at point (n, m) must be changed by

$$\begin{aligned}\psi_r(n,m) =& nd(\sin\varphi_r\cos\phi_r - \sin\varphi\cos\phi)\\ &+ md(\sin\varphi_r\sin\phi_r - \sin\varphi\sin\phi)\end{aligned} \tag{6}$$

The equations above assume that the phase shifts can be controlled continuously. A recent theoretical study has shown that as the number of elements increases, the number of required distinct phase values is reduced [15]. Furthermore, as the number

of elements approaches infinity, only two phase values are needed (1-bit control). For instance, with 300 elements the phase control with 2-bits (4 phase values) reduces the performance by 10% compared with the case where phase is controlled continuously, i.e., not with discrete steps. Additionally, when the number of elements in the array is further reduced to three, three bits are needed translating to eight phase shifts values, given that the reduction in performance from continuous phase control case does not exceed 10% [15].

3.2 Antenna array based RIS in wireless systems

In the RIS aided systems and algorithm development, the elements in the RIS are typically modeled to operate independently of each other, i.e., with no mutual coupling between the elements of the RIS. This means that those theoretical results and algorithms are applicable to antenna array-based reflectors. In addition, in many cases, the reflectors are simply modeled as linear arrays. For performance studies, the array geometry has a negligible impact on the reflection behavior of the RIS. However, the array geometry needs to be considered to apply the algorithms for two-dimensional arrays.

Alternating optimization is used in [16] to find the optimal phase values for the RIS elements and the transmit covariance matrix to maximize the channel capacity of an antenna array based RIS assisted MIMO link. In the numerical examples in [16], a RIS with 20 elements increased the achievable rate performance by 38.8% in a MIMO-OFDM link under frequency-selective channel condition. The use of antenna array based RIS in orthogonal and non-orthogonal multiple access schemes is studied in [17] wherein the capacity and rate regions for both schemes are characterized. Numerical examples show the performance gains achieved by deploying a RIS, e.g, in a two user non-orthogonal multi access scheme the gain in the common average rate is 12 dB. In order to achieve such high gains, a real-time RIS control link is assumed. It is also shown that for practical systems, the phase control resolution in the RIS can be as low as two bits (four phase values for the RIS elements).

The antenna array based model is used in [15] for determining the effect of the phase control resolution on the RIS-assisted links. In [18], a uniform rectangular antenna array model is used in an optimal joint beamforming design for a BS and RIS in a single-cell multi-user network. The RIS in [18] can be switched between two modes. It can be used either for channel estimation or as a steerable beamforming reflector. In a single-user case, the results showed that the signal-to-noise ratio (SNR) increases quadratically with the number of reflecting elements of the RIS. In the multi-user case, it was demonstrated that interference suppression with an RIS can be jointly designed with the access point (AP) transmit beamforming for improving the performance of all users in the system. Furthermore, the wireless network performance can be improved in terms of energy consumption, coverage as well as achievable rate as compared to the conventional systems without using the RIS [18].

In [19], Huang et. al design an antenna array-based RIS system for transmit power allocation as well as for phase shift control single-cell multi-user systems, in which a multi-antenna base station serves single antenna receivers. The methods proposed in [19] are capable of improving the energy efficiency by three-fold in comparison to the conventional multi-antenna amplify-and-forward relaying. In [20], RIS is used to enhance the

communications from a single antenna base station to single-antenna users located within the vicinity of the RIS. The flexibility of joint resource allocation is accomplished by allowing the RIS reflection coefficients to be dynamically tuned over different time slots to create time-varying channels to each user.

In [21], RIS is used as a reflector to enhance the communication link with the aid of beamforming. Additionally, it employs spatial modulation for sending its private data to the receiver. The data sent by RIS is used to control the reflecting elements using the ON and OFF states, where the phase shifts of the elements in the ON state are used for steering the reflected signal. The employed beam steering improves the average SNR at the receiver by up to 9 dB, when average 50% of elements are in active state (RIS size 32×32 elements). Furthermore, a two-step approach is utilized for retrieving the information transmitted from both the transmitter and RIS. The proposed techniques provide a trade-off between the attainable beamforming gain of the reflected signal and the achievable information rate of RIS data.

In [22], the steering of the reflected signal from an intelligent surface is used to enhance the signals for transmission pairs, while canceling the interference from other transmitters. This study also reports measured results as well as the theoretical analysis of the potential gain of the proposed system. The intelligent surface used relies on an (6×8)-element array of controllable patch elements, which are controlled with the aid of varactors. In the measurements, the RIS is used for suppressing the interference. It is shown that the maximum achieved interference suppression reaches around 30 dB, however, in a very narrow bandwidth. For instance, the -20 dB bandwidth is less than 5 MHz and the -10 dB bandwidth is less than 10 MHz. The results show that the controllable surface can be used for interference mitigation.

The array design in [20] is based on a reflector array described in [12]. More specifically, the reflect array designed and implemented in [12] consists of 70 elements that operate at 5.8 GHz. The array is capable of steering the incident beam angle between -50° to $+50^\circ$ from the array normal with 5° steps. The total signal loss in the system is 7.4 dB, which is caused by the feed efficiency. Particularly, the loss due to element absorption, phase error and element factor are reported to be 1.8 dB, 0.8 dB and 0.8 dB, respectively.

A RIS prototype with 256 elements has been published in [23]. The phase shifts of the RIS elements in [23] are controlled with two-bits and it achieves a 23 dBi antenna gain at 2.3 GHz. The physical size of the RIS prototype is 0.8 m $\times$ 0.8 m. The -1 dB bandwidth is 350 MHz and the beam can be scanned from 0° to 60° from the broadside of the RIS.

Many of the articles considering the algorithms to control the RIS use the MIMO type processing [18, 19, 21], where the channel is first estimated, and the beam steering and the radio resource management is based on the estimated channel state information. A different approach is proposed in [24], where no channel estimation is needed to control the reflection. Therein the reflecting surface used 3200-elements antenna array with an area of array 6 m^2. The control of the array is implemented with a majority voting algorithm. In the training phase, the array is randomly configured to states where some of the elements reflect the incident signal and others do not. The receiver reports the received power at different stages of the training to the network. After K measurements, the median of the received power is calculated. Specifically, if the received power

is above the median more often when element i has been active than when it has been switched off, the element i is voted to be on. Otherwise it is voted to be off. The training of the surface requires no changes to the signal processing in the transceivers. Furthermore, the received power level is reported with the received signal strength indicator (RSSI), which is commonly available in essentially all wireless communication systems. The RSSI information is reported to the control unit of the reflecting surface. In the test scenarios, the receiver is kept at the same position close to the surface, while the position of the transmitter is altered. The SNR gain in these experiments spans from 3.8 to 20 dB with a median of 9.5 dB.

4 Metasurfaces in RIS applications

4.1 Metasurface

In antenna array based RIS, the structure of the radio surface is fixed, which imposes a limited control on the RIS. However, metasurfaces, which are electrically thin and dense two-dimensional arrays of structural elements possessing the desired properties granted by their constitutive elements, allow a more flexible control on the operation of RIS. More specifically, the metasurface can be designed as a cluster of basic elements (colored elements in the top part of Fig. 3), where the operation of a single element is designed based on the requirements set on the operation of RIS. Alternatively, it can be designed as a collection of sub-areas, as depicted in the bottom part of Fig. 3. Hence, the granularity of the control spans from hundreds or thousands controllable elements (depending on the metasurface size) to the case where a whole RIS is a single area with one controllable state, e.g., surface reflects or absorbs the incoming wave. The signal reflected by a meta-surface can also be described with (1)–(6) assuming that the elements of the metasurface have been fixed, or in the case of controllable metasurface, after the state of the controllable elements have been changed. However, in a metasurface, the dimensions and spacing between the elementary elements (called unit cells, meta cells, meta atoms, etc.) are much smaller than the wavelength of the EM wave to be controlled (typically between $\lambda/10$ and $\lambda/5$) [8, 9]. This means that in the design phase, a metasurface cannot be modeled as an antenna array, but instead the analysis and design of metasurfaces can be based on the concept of polarizability.

By distributing unit cells with different polarizations, the reflection and refraction can be realized to other directions according to the generalized Snell's law defined by (7). The polarizability of a unit cell can be controlled by the cell's size and shape as well as by its inter-spacing distance from neighboring unit cells. This approach is used in the design of fixed metasurfaces. A more detailed description of the connection between the polarizabilities of unit cells and the desired directions of refraction and can be found in [25]. A controllable metasurface can be implemented with identical unit cells distributed evenly on the surface, where their polarizability can be controlled. This can be realized by connecting the meta cells (metal patches in Fig. 5) to each other or to the ground with a varactor in the same manner as in antenna array-based RIS.

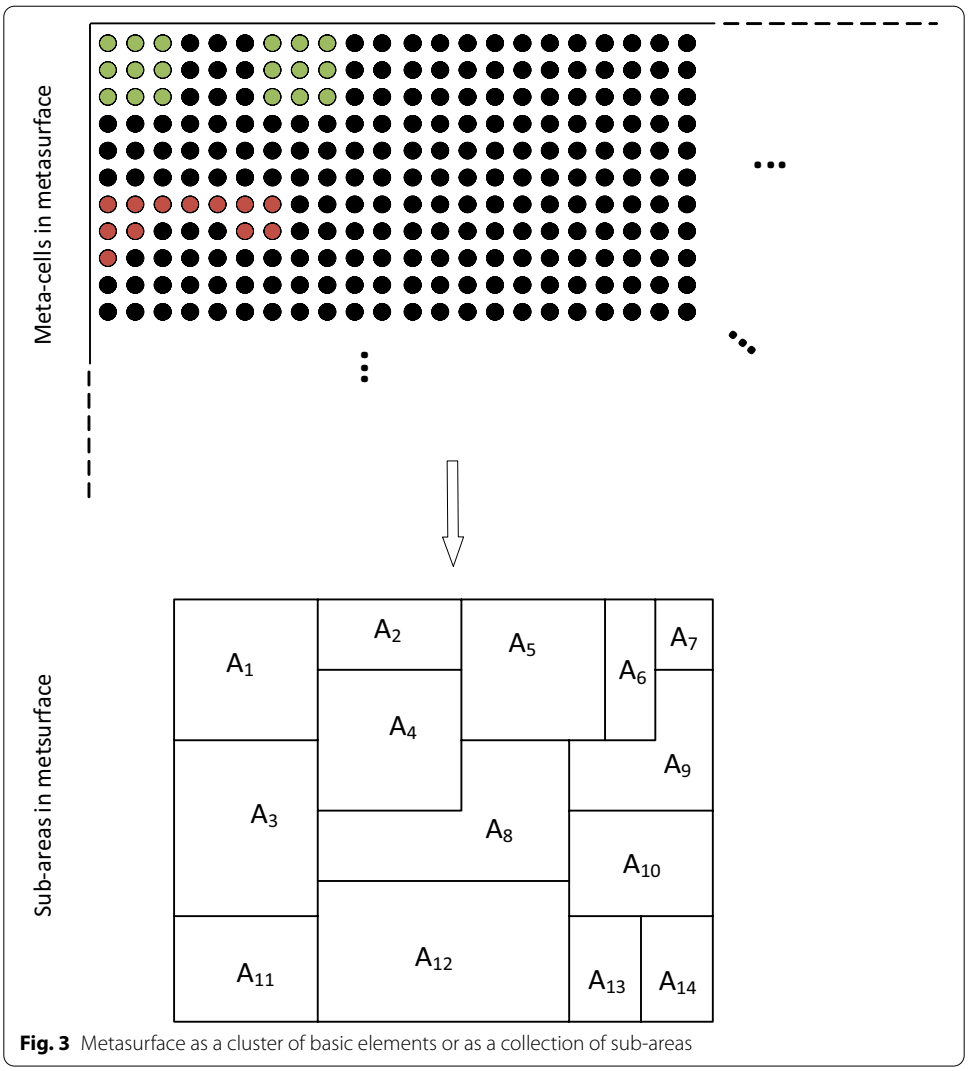

Fig. 3 Metasurface as a cluster of basic elements or as a collection of sub-areas

4.2 Reflection and refraction in metasurfaces

The Snell's law relates the incident angle with the angle of refraction, i.e., the change in the EM propagation direction (see Fig. 4b), at the boundary of two dielectric materials and it can be written as

$$\upsilon_2 \sin\theta_t = \upsilon_1 \sin\theta_i \tag{7}$$

where, θ_i is the incident angle and θ_t is the angle of refraction, while υ_1 and υ_2 are the refractive indices of the materials where the EM wave is arriving to the boundary between the two materials (material 1) and the material where the EM is propagating after the refraction (material 2), respectively. In the case of reflection, the reflection angle (θ_r) from the same boundary is the same as the incident angle, i.e., $\theta_r = \theta_i$. The above states that the angles of the reflection and refraction depend only on the material properties at both sides of the boundary between the materials and the incident angle of the EM wave. The boundary between the two materials does not allow to steer the

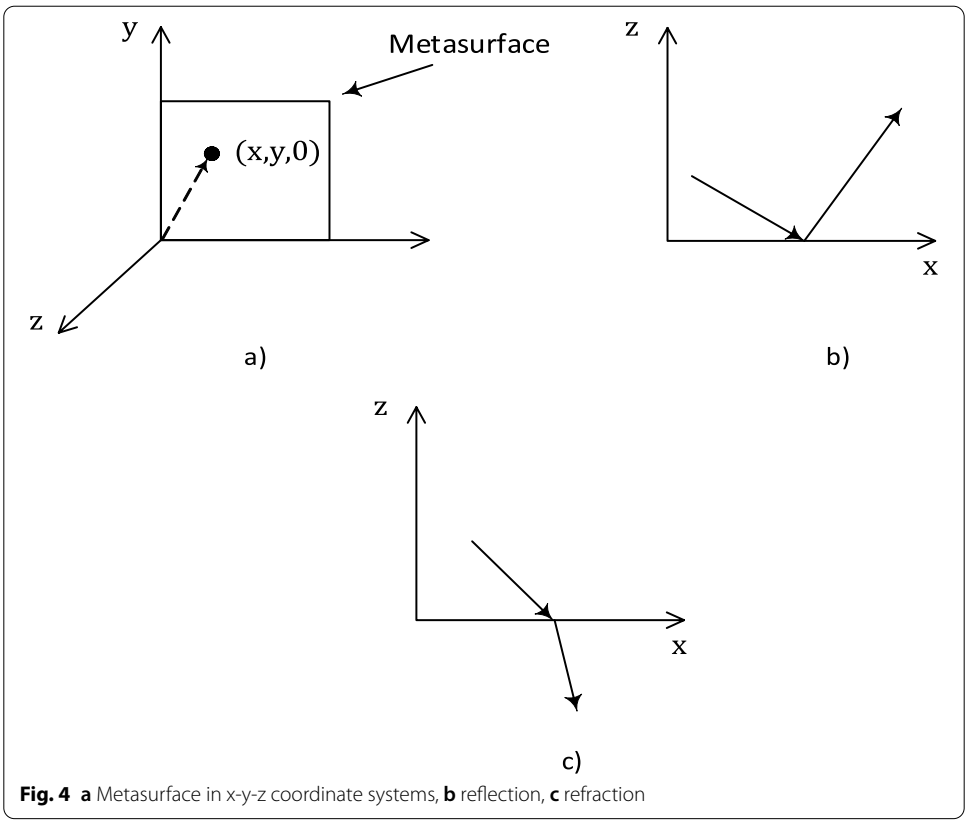

Fig. 4 **a** Metasurface in x-y-z coordinate systems, **b** reflection, **c** refraction

EM waves to any other directions. However, when an appropriately designed thin sheet is placed between the two materials, it is possible to control the behavior of the EM waves above and below the sheet more freely [25–29]. The engineered thin sheets with designed reflective, refractive and absorption properties are called metasurfaces.

A metasurface is shown in Fig. 4a in the $x-y-z$ coordinate systems. It can be designed to reflect the impinging EM wave. The reflecting wave then propagates in the same medium where it propagated before the reflection, but the propagation direction has changed. The EM wave arriving from the direction defined by the x and z coordinates is shown in Fig. 4b. The relation between the reflection and incidence angles in the case of metasurfaces can be written as

$$\upsilon_1(\sin\theta_1 - \cos\theta_r) = \frac{\partial\phi_r(x,y,0)}{\partial x} \tag{8}$$

where $\phi_r(x,y,0)$ is the phase of the reflection coefficient at point $(x, y, 0)$. If the propagation direction of EM is defined in the $y-x$ plane, the partial derivative in (8) is calculated with the respect to y. Other directions can be calculated as the superposition of these two.

When metasurfaces are used to implement an RIS, the design goal in addition to control the direction of reflection, is to maximize the reflected power to the desired direction.

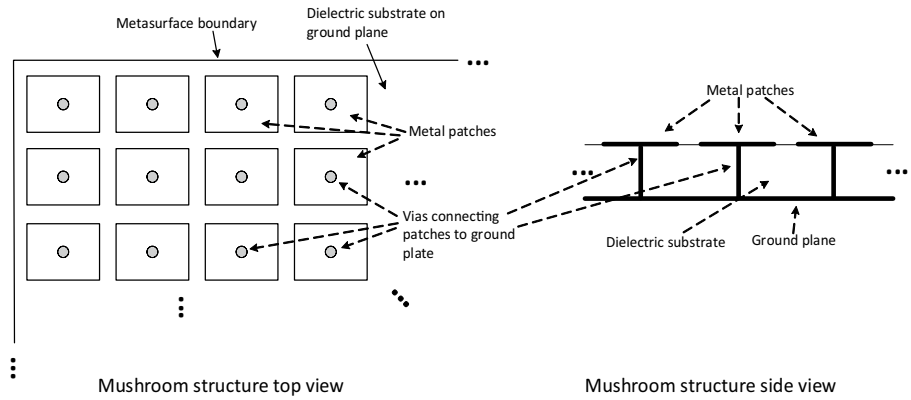

Fig. 5 Top and side view of mushroom structure

4.3 Controllable metasurfaces

Often used structure to implement a configurable of tunable metasurface is the mushroom structure portrayed in Fig. 5. It consists of rectangular small metal patches placed close to each other on a thin dielectric substrate. At the other side of the substrate is the ground plane. The patches of Fig. 5 are connected to the ground plane by vias going through the dielectric substrate.

Metasurfaces and similar electrically thin structures have been used for a long time to control the propagation of EM waves. In communication applications, these designs have been used especially in antenna designs. Most of the metasurfaces are fixed. They are designed to steer the EM wave coming from a known direction to the predetermined directions. A comprehensive review of metasurfaces can be found in [3]. It covers the applications and technologies of metasurfaces from microwave to optical frequencies.

In metasurface based RIS applications, the properties of the metasurface must be controllable. The incident field must be directed to directions where the receiving nodes are in order to improve the performance of a communication or positioning system. A review of the state-of-the-art on controllable metasurfaces is presented in this section. The implementations described below represent the typical published designs. The frequency range of interest in this survey is 2–10 GHz.

The programmability or tunability of metasurface based RISs requires the integration of active elements with the unit cells of the metasurfaces. Controlling the microwave frequencies can be realized with the aid of varactors. A common implementation technique of varactors uses p-i-n diodes as in [30]. At higher frequencies (terahertz to optical frequencies) tunability can be realized with, e.g., transparent conductive oxides, ferroelectric materials, liquid crystal, graphene and phase change materials [31]. Graphene has also been used to implement a tunable absorber working at 3.41–4.55 GHz in [32]. Since the considered application is RIS and the frequency range in interest in this work is below 10 GHz, these are not considered here.

A metasurface for electrically controlled beam steering was introduced in [30]. The structure of the metasurface consists of small square metal patches on a dielectric substrate. Patches are connected to the ground plate using a via. This kind of structure is commonly called a mushroom structure and it is illustrated in Fig. 5. Each patch is

connected to its adjacent patches by a varactor. By changing their control voltages, the resonant frequency of the unit cells (patches with vias) can be varied. By adjusting the resonant frequency of the unit cells, the phase of the reflection coefficient at different points on the metasurface can be controlled. This allows to create the required phase gradient to steer the reflected EM wave. The reflection can be controlled in two dimensions (both azimuth and elevation planes). The designed metasurface in [30], is operating at 3.5 to 5.0 GHz frequency and is able to steer the incident beam over $\pm 40^\circ$ from the surface normal. The reported main beam width and gain are 15° and 14 dBi, respectively. Maximum sidelobes are -10 dB below the maximum gain of the radiation pattern and the bandwidth is about 8% at 4.5 GHz ($\approx$ 360 MHz).

The control of the reflection in [30] is based on analog signal processing, the reflection direction is changed by changing the bias voltages of the varactors. The reflection from a metasurface can be controlled also digitally. A digitally controllable structure based on the similar mushroom structure as in [30] has been considered in [33]. The varactor is connected between the metal patch and the ground plate in [33] and not between the patches as in [30]. The varactor bias line design allows the beam steering only in one dimension. The control is implemented with a field programmable array (FPGA), varactors can be programmed to be in two states, "ON" or "OFF". The implementation in [33] is designed for 10 GHz center frequency. The maximum diode switching speed is 5 MHz. The control voltage is used to change the operating frequency around the center frequency as well as the reflection direction, i.e., beams pointing into different directions are at different frequencies. The range of the beam steering control is between 45° and 50°.

Metasurface controlled by an FPGA is considered also in [34]. By changing the state of the diode between "0" and "1", the reflection coefficient of the unit cell is changed between 0° and 180°. By properly selecting the control bit pattern on the surface, the reflection can be directed to desired directions. The prototype consists of 30×30 unit cells.

An FPGA controlled reflective metasurface is described also in [35]. The control of the surface is implemented by switching the diode "ON" or "OFF" as in [33, 34]. The implemented metasurface consists of an array of 20×20 unit cells. The operating frequency is 3.5 GHz. The same unit cell structure is used also in [36]. Instead of controlling the bias voltage digitally, the control is realized with light. By changing the intensity of the light illuminating the surface, the bias voltages of the varactors can be switched "ON" or "OFF" with photodiodes. The control of the metasurface by switching the varactor diodes "ON" or "OFF" is used also in [37]. The metasurface can be used for generating multi-ple beams or twin-beam scanning in the low frequency band around 6 GHz while dynamic beam-scanning in high frequency band at 9.8 GHz.

In [38], the varactors are used to tune the operating frequency of the metasurface between 4.1. and 6.6 GHz. Varactors are used only for the frequency tuning, not to direct the reflection.

A metasurface based on a more complex unit cell is described in [39]. The structure consists of a parallel LC resonant circuit and small metallic loops. Varactors integrated into the unit cell allow the dynamic tuning of the surface impedance of the surface. The design in [39] is used to control the refraction, i.e., the EM wave traveling through the

surface, and not the reflection. The implemented prototype operates at 3 GHz frequency. The transmittivity of the surface can be tuned from 0 to 1 when the phase of the EM wave is kept unaltered, or the phase of the transmission can be tuned by 360° while the transmittivity is kept constant. In [39], the control of the refraction angle itself is not demonstrated. But if different areas (unit cells) of the surface are programmed to induce different phase shifts of the EM wave, the refraction direction can, in principle, be controlled.

In [40], unit cells are realized with two twisted square split ring resonators to implement a tunable chiral metasurface. The surface is designed to act as a lens capable to steer the EM wave propagating through it and its operating frequency range is 8–10 GHz. About 80% of the incident power is transmitted through the surface. The tuning of the surface is done with varactors.

The application discussed in [41] is an antenna array design. The results illustrate the ability of a metasurface to steer the EM wave propagating through it (microwave lens). The scanning range of an antenna array is increased from [− 36°, 38°] to [− 56°, 60°] with the usage of the metasurface design but the gain in main lobe direction is reduced due to losses in the metasurface. The transmittivity of the surface is above 0.8 from 9 GHz to 10 GHz. The unit cell in [41] is based on a sandwich structure, where the top and bottom layers are co-centric combinations of square ring and circular patches.

The design in [42] is used to implement an absorber around 3.6 GHz frequency. It is not directly applicable to be used in RIS applications, but is included here because of its control circuitry design. In most of the tunable/controllable metasurface designs below 10 GHz, the tuning is implemented with lumped components (varactors). The tuning is accomplished by changing the bias voltage of the varactors. The unit cell designed with metal-oxide-semiconductor field-effect transistors in [42] enables the control of not only the capacitance but both the real and imaginary part (resistance and reactance) of the loading impedance.

The tunability of the metasurface in [43] is proposed to be implemented using mixed signal integrated circuit embedded in the unit cell. The IC connects two metal patches of the unit cell to enable the control of unit cell resistance and reactance. This offers the local control over the surface resulting in the control of the reflection properties. The operation of the concept is verified by a design operating at 5 GHz frequency. The performance of the design is studied with simulations. The IC proposed for the tuning it not designed but its operation is modeled as a continuously tunable, lumped complex tunable impedance.

4.4 Metasurface based RIS in wireless systems

The scenario used in [9] and [44] is an indoor wireless communication environment in which the interior walls of the building are fully covered with metasurfaces. Users inside the building require different services simultaneously, some of the users want to have optimal connectivity, others may require protection from eavesdropping and some users are interested in wireless power transfer. In addition, interference and unauthorized connection from outside the building are blocked by the system. The main parts of [9] and [44] describe a general framework for software interface architecture for the control of the envisioned system. The metasurfaces are assumed to be almost ideal, i.e., it

is assumed that metasurfaces do not exhibit any major limitations regarding the electromagnetic functionalities that they can support.

In [45, 46], interior wall of a building is assumed to be covered by a surface whose EM properties can be switched between two states. In one state, the EM wave can propagate through the wall, in the other state the wall attenuates the EM wave propagating from one room to the next through the wall. This can be used to decrease the interference between local networks operating in adjacent rooms or to deny access to the local network from outside the room. The system model in [45, 46] is much simpler than the one in [44], but it is also more realistic in the sense that it does not require ideal configurable surface. In the simulation case, it is assumed that when the signal is allowed to propagate through the wall it is attenuated by 2 dB and when the wall is configured to attenuate the signal, the attenuation is 25 dB.

According a Press Release [47], NTT DOCOMO has demonstrated the control of EM propagation through a window using a metasurface operating at 28 GHz. Although this test was conducted at a frequency range above our focus, it has been included, because it is the first test of metasurface based RIS application published by one of the major operators.

A different kind of application of a metasurface in wireless communications is demonstrated in [48]. The reflecting metasurface is used for data modulation. In the proposed transmitter architecture, a feed antenna transmits a carrier wave to the metasurface. The reflection coefficient of the metasurface is controlled with the transmitted baseband data signal resulting in a modulated signal at the radio frequency. The center frequency in the test has been 4 GHz and QPSK is used for the data modulation. The achieved data rate is 2.048 Mbps with a single carrier modulation. The benefit of using the metasurface as a transmitter is that the up-conversion based on mixers used in conventional transmitters is omitted. The disadvantage is the power loss. In [48], the conventional transmitter requires 5 dB less power than the one based on the metasurface modulator.

5 Results and discussion

The potential use cases and the benefits of the RIS at frequencies below 10 GHz are still not fully known. The results from prototypes reviewed in this survey indicate that a RIS can be used to control the EM propagation also at this frequency range. An EM wave is attenuated, when it reflects from floors, walls, and ceilings. The reflection attenuation of typical construction materials is in the order of 7–10 dB. This implies that there are typically few dominant directions where the signal arrives from at any point. This is also visible in typical measurement-based channel models, e.g., in 5G channel models [49]. Although the dominant channel direction below 10 GHz is not as clear as at higher frequencies (tens or hundreds GHz), a RIS has potential to extend the coverage and increase the channel capacity. However, channel measurements for RIS assisted systems operating at the sub-gigahertz frequency range are needed to verify the potential gains.

Intelligent radio surfaces below 10 GHz frequency can be implemented with antenna arrays or metasurfaces. The electromagnetic theories and models for the analysis and design for both options are well known and commercial simulation tools for modeling are available. The exact theoretical model for a large complex structure can, in principle, be formed, but in practical work the design is done with design and simulation tools.

This is evident also in publications reporting the designed, simulated, and implemented metasurfaces. Design with simulation tools can be efficient, but the development of control algorithms for metasurface based RIS necessitates models for the metasurface operation. The properties of the metasurfaces, e.g. the surface impedance, depends on the polarization and the angle-of-arrival (both azimuth and elevation) of the impinging electromagnetic wave. Further, the unit-cells of the metasurface are mutually coupled to their neighbouring cells. Accurate models for these effects are not yet available for control algorithm development.

Unit cells used for the reconfigurable metasurfaces below 10 GHz frequency are mostly based on simple geometrical shapes such as rectangular patches, H-shape, and rectangular rings. The sizes of the implemented surfaces are in the order of 30×30 unit cells (about 30 cm $\times$ 30 cm). The materials used are the same as those used in printed circuit boards at microwave frequencies. More exotic materials and complex unit cell structures are used at higher frequencies, terahertz and optical frequencies. The reflectivity and transmittivity of the prototypes are below 0.9 (10% or more loss). The tuning is implemented typically with varactors. In published antenna array model based algorithm designs, the elements of the arrays are assumed to operate independently (no mutual coupling between elements) and the phase control is assumed to be implemented in the same manner as in the antenna arrays. While in the conventional antenna array cases the phase of the transmitted (or received) signal can be controlled with phase shifting circuits, in reflect arrays the phase shift must be done by changing the physical properties of the elements, namely, the resonance frequency. If the number of elements in a reflect array is large, the control of RIS can be realized by switching the phase response of the elements between distinct values, i.e., the phase control does not need to be continuous. The unit-cells are close to each other in metasurfaces, which means that they cannot be assumed to operate independently. In addition, the number of controllable elements can be much higher than in the reflect array based designs. In the published demonstrations of controllable metasurfaces, the operation of unit-cells has had two states. In some cases, the allowable unit-cell states are ON or OFF. In other cases, the unit-cell reflection angle has had two distinct values. The details of the algorithms have not been published.

In addition to the theoretical works, some tests and demonstrations of metasurface based intelligent radio surfaces in wireless systems have been published. The most complete demonstrations are probably the ones performed by NTT DOCOMO in Japan. Unfortunately, only press releases with restricted information content on these were found. Other published tests show that it is possible to improve the performance of a wireless system by using the controllable reflecting surfaces, but the available information is insufficient to assess the gain in practical scenarios with complete wireless systems based on the published results so far.

Commercial products based on the metasurfaces are mainly transmit/receive antennas. Some of the companies have commercial-off-the-shelf antenna products, but these companies are mainly design houses offering design services for metasurface based products. The feasibility of using fixed reflecting surfaces to improve the coverage and service quality of wireless communication has been already demonstrated, especially by the experiments by DOCOMO in Japan. Theoretical studies have already showed that surfaces with controllable properties can further enhance the performance of wireless

Table 1 Comparison of metasurface and reflectarray based RIS

Relectarray	Metasurface
Operation well-known, relatively easy to model	Difficult to model controllable surfaces
Simple to manufacture	Potentially more advanced functions
Simple control	Mutual coupling of meta-cells complicates the control
Readily available technology	Reconfigurable metasurfaces still in research phase

systems. New, improved services, such as accurate positioning and improved information security, have been envisioned and some initial published studies support this assumption. However, to fully understand the benefits the intelligent radio surfaces can bring, more extensive investigations on the possible use cases needs to be done.

Controllable surfaces can be implemented with conventional reflect arrays, but metasurface based structures can offer more extensive options for the control. The operation of fixed metasurfaces is known and some controllable or tunable metasurfaces have been designed and implemented. Published controllable metasurfaces are relatively small and their electromagnetic properties (reflection efficiency, beam width, steering range and accuracy, etc.) have not yet been thoroughly studied. The research on the control of the intelligent surfaces, i.e., system architecture and algorithms, is in early stages. Algorithms published so far apply techniques used in the MIMO systems. While this approach can provide good results with relatively small antenna array based surfaces, the efficient control of large reflect arrays may require new approaches. The large numbers of controllable elements and their strong mutual coupling in metasurfaces require deviation from the MIMO processing-based approach. The efficient control of metasurface based intelligent surfaces is largely an open problem. The comparison of a reflectarray and a metasurface as a RIS implementation technology is summarized in Table 1.

Abbreviations

AP: Access point; dB: Decibel; dBi: Decibel isotropic; EM: Electromagnetic; FPGA: Field programmable gate array; FR1: 5G NR frequency range 1; GHz: Gigahertz; IC: Integrated circuit; IRS: Intelligent reflecting surface; LC: inductor-capacitor; LIS: Large intelligent surface; MHz: Megahertz; NR: New radio; QPSK: Quadrature phase shift keying; RIS: Reconfigurable intelligent surface; MIMO: Multiple-input multiple-output; RF: Radio frequency; RX: Receiver; THz: Terahertz; TX: Transmitter.

Acknowledgements

Not applicable.

Author contributions

All authors have contributed to the literature search and to the writing of the survey. All authors read and approved the final manuscript.

Authors' information

Visa Tapio received his M.Sc. (EE) and Lic.Sc. (EE) degrees from University of Oulu, Oulu, Finland in 1995 and 2004, respectively. V. Tapio has been with University of Oulu since 1994. His research interests include the wireless transceiver development, especially the relation between the physical characterization of transceivers at radio frequencies and digital signal processing algorithm.

Ibrahin Hemadeh is an R&D staff engineer at Interdigital. He received his MSc degree (Hons.) in wireless communications and his PhD degree in electronics and electrical engineering from The University of Southampton, UK, in 2012 and 2017, respectively. In 2017, he joined the Southampton Next Generation Wireless Group, The University of Southampton, as a Post-Doctoral Researcher. In 2018, he joined the 5G Innovation Centre (5GIC) at the University of Surrey. His research interests include reconfigurable intelligent surfaces, millimeter-wave communications, multi-functional multiple input multiple output (MIMO), multi-dimensional (time-space and frequency) transceiver designs, channel coding, as well as multi-user MIMO.

Alain Mourad is a Director Engineering R&D at InterDigital Labs in London (UK) leading research on 5G and beyond. Prior to InterDigital, Alain was a Principal Engineer at Samsung Electronics R&D and previously a Senior Engineer at Mitsubishi

Electric R&D Centre Europe where he was active in the specification of wireless standards (3GPP, IEEE802, DVB, ATSC). Alain is a prolific inventor with over 50 issued patents. He received Samsung Electronics Inventor Awards in 2012 and 2013, InterDigital Awards in 2016, 2018 and 2020, and 2018 Global Telecoms Awards "Highly Commended" for "Advancing the road to 5G".

Arman Shojaeifard has +7 years of work experience in research and development of air-interface technologies and architectures for 4G LTE/LTE-A, 5G NR, and beyond. He received the BEng degree in Information Systems Engineering from Imperial College London in 2008. He then graduated from King's College London in 2009, with an MSc degree in Signal Processing (with Distinction), and in 2013, with a PhD degree in Wireless Communications. He is currently a Staff Engineer at InterDigital where he leads the CELTIC-NEXT European collaborative project on AIMM (AI-enabled Massive MIMO). He was previously a Wireless Research Manager and 3GPP RAN1 WG Delegate at British Telecoms. Prior to that, he held post-doctoral research positions at University College London and University of Manchester. He is currently an Editor for IEEE Wireless Communications Letters and IET Electronics Letters.

Markku Juntti received his Dr.Sc. (EE) degree from University of Oulu, Oulu, Finland in 1997. Dr. Juntti was with University of Oulu in 1992–98. In academic year 1994–95, he was a Visiting Scholar at Rice University, Houston, Texas. In 1999–2000, he was a Senior Specialist with Nokia Networks, Oulu, Finland. Dr. Juntti has been a professor of communications engineering since 2000 at University of Oulu, Centre for Wireless Communications (CWC), where he also serves as Head of CWC – Radio Technologies Research Unit. His research interests include signal processing for wireless networks as well as communication and information theory. Dr. Juntti is also an Adjunct Professor at Rice University.

Funding
The research by V. Tapio and M. Juntti has been funded in part by InterDigital Corporation and the Academy of Finland 6Genesis Flagship (grant 318927).

Availability of data and materials
Data sharing is not applicable to this article as no datasets were generated during the current study.

Declarations

Competing interests
The authors declare that they have no competing interests.

Author details
[1]Centre for Wireless Communications, University of Oulu, Oulu, Finland. [2]InterDigital Europe, Ltd, London, UK.

Received: 8 April 2021 Accepted: 1 September 2021
Published online: 10 September 2021

References

1. M. Di Renzo, A. Zappone, M. Debbah, M.-S. Alouini, C. Yuen, J. de Rosny, S. Tretyakov, Smart radio environments empowered by reconfigurable intelligent surfaces: How it works, state of research, and the road ahead. IEEE J. Sel. Areas Commun. **38**(11), 2450–2525 (2020). https://doi.org/10.1109/JSAC.2020.3007211
2. E. Basar, M. Di Renzo, J. De Rosny, M. Debbah, M. Alouini, R. Zhang, Wireless communications through reconfigurable intelligent surfaces. IEEE Access **7**, 116753–116773 (2019). https://doi.org/10.1109/ACCESS.2019.2935192
3. Q. Wu, R. Zhang, Towards smart and reconfigurable environment: intelligent reflecting surface aided wireless network. IEEE Commun. Mag. **58**(1), 106–112 (2020). https://doi.org/10.1109/MCOM.001.1900107
4. N. Rajatheva, White paper on broadband connectivity in 6G. Technical report, Finnish 6G Flagship Program (2020). http://jultika.oulu.fi/files/isbn9789526226798.pdf
5. H. Wymeersch, J. He, B. Denis, A. Clemente, M. Juntti, Radio localization and mapping with reconfigurable intelligent surfaces: challenges, opportunities, and research directions. IEEE Veh. Technol. Mag. **15**(4), 52–61 (2020). https://doi.org/10.1109/MVT.2020.3023682
6. C. de Lima, et al. 6G white paper on localization and sensing. Technical report, Finnish 6G Flagship Program (2020). http://jultika.oulu.fi/files/isbn9789526226743.pdf
7. M. Di Renzo, et. al. Smart radio environments empowered by reconfigurable AI meta-surfaces: an idea whose time has come. J. Wirel. Com Network 2019, 129 (2019) (2019). https://doi.org/10.1186/s13638-019-1438-9
8. S.B. Glybovski, S.A. Tretyakov, P.A. Belov, Y.S. Kivshar, C.R. Simovski, Metasurfaces: from microwaves to visible. Phys. Rep. **634**, 1–72 (2016). https://doi.org/10.1016/j.physrep.2016.04.004
9. C. Liaskos, S. Nie, A. Tsioliaridou, A. Pitsillides, S. Ioannidis, I. Akyildiz, A novel communication paradigm for high capacity and security via programmable indoor wireless environments in next generation wireless systems. Ad Hoc Netw. **87**, 1–16 (2019). https://doi.org/10.1016/j.adhoc.2018.11.001
10. T. Nakanishi, T. Otani, Y. Tamayama, M. Kitano, Storage of electromagnetic waves in a metamaterial that mimics electromagnetically induced transparency. Phys. Rev. B **87**, 116110 (2013). https://doi.org/10.1103/PhysRevB.87.161110
11. A. Silva, F. Monticone, G. Castaldi, V. Galdi, A. Alù, N. Engheta, Performing mathematical operations with metamaterials. Science 343(6167), 160–163 (2014). https://doi.org/10.1126/science.1242818
12. S.V. Hum, M. Okoniewski, R.J. Davies, Modeling and design of electronically tunable reflectarrays. IEEE Trans. Antennas Propag. **55**(8), 2200–2210 (2007). https://doi.org/10.1109/TAP.2007.902002
13. C.A. Balanis, *Antenna Theory: Analysis and Design*, 2nd edn. (Wiley, 1997)

14. R. Garg, I.I.P. Bhartia, *Microstrip Antenna Design Handbook* (Artech House, Inc., 2001)
15. H. Zhang, B. Di, L. Song, Z. Han, Reconfigurable intelligent surfaces assisted communications with limited phase shifts: how many phase shifts are enough? IEEE Trans. Veh. Technol. **69**(4), 4498–4502 (2020). https://doi.org/10.1109/TVT.2020.2973073
16. S. Zhang, R. Zhang, Capacity characterization for intelligent reflecting surface aided MIMO communication. IEEE J. Sel. Areas Commun. **38**(8), 1823–1838 (2020). https://doi.org/10.1109/JSAC.2020.3000814
17. X. Mu, Y. Liu, L. Guo, J. Lin, N. Al-Dhahir, Capacity and optimal resource allocation for IRS-assisted multi-user communication systems. IEEE Trans. Commun. **69**(6), 3771–3786 (2021). https://doi.org/10.1109/TCOMM.2021.3062651
18. Q. Wu, R. Zhang, Intelligent reflecting surface enhanced wireless network via joint active and passive beamforming. IEEE Trans. Wireless Commun. **18**(11), 5394–5409 (2019). https://doi.org/10.1109/TWC.2019.2936025
19. C. Huang, A. Zappone, G.C. Alexandropoulos, M. Debbah, C. Yuen, Reconfigurable intelligent surfaces for energy efficiency in wireless communication. IEEE Trans. Wireless Commun. **18**(8), 4157–4170 (2019). https://doi.org/10.1109/TWC.2019.2922609
20. Y. Yang, S. Zhang, R. Zhang, IRS-enhanced OFDMA: Joint resource allocation and passive beamforming optimization. IEEE Wireless Commun. Lett. **9**(6), 760–764 (2020). https://doi.org/10.1109/LWC.2020.2968303
21. W. Yan, X. Yuan, X. Kuai, Passive beamforming and information transfer via large intelligent surface. IEEE Wireless Commun. Lett. **9**(4), 533–537 (2020). https://doi.org/10.1109/LWC.2019.2961670
22. X. Tan, Z. Sun, J.M. Jornet, D. Pados, Increasing indoor spectrum sharing capacity using smart reflect-array. In: 2016 IEEE International Conference on Communications (ICC), pp. 1–6 (2016). https://doi.org/10.1109/ICC.2016.7510962
23. L. Dai, B. Wang, M. Wang, X. Yang, J. Tan, S. Bi, S. Xu, F. Yang, Z. Chen, M.D. Renzo, C.-B. Chae, L. Hanzo, Reconfigurable intelligent surface-based wireless communications: antenna design, prototyping, and experimental results. IEEE Access **8**, 45913–45923 (2020). https://doi.org/10.1109/ACCESS.2020.2977772
24. V. Arun, H. Balakrishhnan, Rfocus: beamforming using thousands of passive antennas. In: USENIX Symposium on Networked Systems Design and Implementation (NSDI '20) (2020)
25. V.S. Asadchy, M. Albooyeh, S.N. Tcvetkova, A. Díaz-Rubio, Y. Ra'di, S.A. Tretyakov, Perfect control of reflection and refraction using spatially dispersive metasurfaces. Phys. Rev. B **94**, 075142 (2016). https://doi.org/10.1103/PhysRevB.94.075142
26. Y. Vahabzadeh, N. Chamanara, K. Achouri, C. Caloz, Computational analysis of metasurfaces. IEEE J. Multiscale Multiphysics Comput. Tech. **3**, 37–49 (2018). https://doi.org/10.1109/JMMCT.2018.2829871
27. E.F. Kuester, M.A. Mohamed, M. Piket-May, C.L. Holloway, Averaged transition conditions for electromagnetic fields at a metafilm. IEEE Trans. Antennas Propag. **51**(10), 2641–2651 (2003). https://doi.org/10.1109/TAP.2003.817560
28. S. Tretyakov, *Analtical Modeling in Applied Electromagnetics* (Artech House, Inc., 2003)
29. K. Achouri et al., Synthesis of electromagnetic metasurfaces: principles and illustrations. EPJ Appl. Metamat. **2**, 12 (2015). https://doi.org/10.1051/epjam/2015016
30. D.F. Sievenpiper, J.H. Schaffner, H.J. Song, R.Y. Loo, G. Tangonan, Two-dimensional beam steering using an electrically tunable impedance surface. IEEE Trans. Antennas Propag. **51**(10), 2713–2722 (2003). https://doi.org/10.1109/TAP.2003.817558
31. L. Bao, T.J. Cui, Tunable, reconfigurable and programmable metamaterials. Microw. Opt. Technol. Lett. **62**(1), 9–32 (2020)
32. J. Zhang et al., Two-dimensional beam steering using an electrically tunable impedance surface. ACS Photonics **7**(1), 265–271 (2020)
33. J. Zhang et al., Space–time-coding digital metasurfaces. Nat. Commun. **9**, 1–11 (2018)
34. T.J. Cui et al., Coding metamaterials, digital metamaterials and programmable metamaterials. Light Sci. Appl. **3**, 1–9 (2014)
35. S. Tian, H. Liu, L. Li, Design of 1-bit digital reconfigurable reflective metasurface for beam-scanning. Appl. Sci. **7**(9), 1–8 (2017)
36. X.G. Zhang et al., Light-controllable digital coding metasurfaces. Appl. Sci. **5**(11), (2018)
37. N. Zhang, K. Chen, Y. Zheng, Q. Hu, K. Qu, J. Zhao, J. Wang, Y. Feng, Programmable coding metasurface for dual-band independent real-time beam control. IEEE Journal on Emerging and Selected Topics in Circuits and Systems **10**(1), 20–28 (2020). https://doi.org/10.1109/JETCAS.2020.2973310
38. H.-X.Xu et al., Tunable microwave metasurfaces for high-performance operations: dispersion compensation and dynamical switch. Sci. Rep. **6**, 38255 (2016). https://doi.org/10.1038/srep38255
39. B. Zhu et al., Tunable microwave metasurfaces for high-performance operations: dispersion compensation and dynamical switch. Sci. Rep. **4**, 4971 (2014). https://doi.org/10.1038/srep04971
40. K. Chen, G. Ding, J. Zhao, Y. Feng, Dynamic control of microwave with tunable metamaterial and metasurface. In: 2018 IEEE Asia-Pacific Conference on Antennas and Propagation (APCAP), pp. 285–286 (2018). https://doi.org/10.1109/APCAP.2018.8538097
41. Y. Lv, X. Ding, B. Wang, D.E. Anagnostou, Scanning range expansion of planar phased arrays using metasurfaces. IEEE Trans. Antennas Propag. **68**(3), 1402–1410 (2020). https://doi.org/10.1109/TAP.2020.2967276
42. K.M. Kossifos, M.A. Antoniades, J. Georgiou, Integrated-circuit enabled adaptive metasurface absorber with independent tuning of orthogonal polarization planes. IEEE Access **8**, 50227–50235 (2020). https://doi.org/10.1109/ACCESS.2020.2977852
43. F. Liu, O. Tsilipakos, A. Pitilakis, A.C. Tasolamprou, M.S. Mirmoosa, N.V. Kantartzis, D.-H. Kwon, J. Georgiou, K. Kossifos, M.A. Antoniades, M. Kafesaki, C.M. Soukoulis, S.A. Tretyakov, Intelligent metasurfaces with continuously tunable local surface impedance for multiple reconfigurable functions. Phys. Rev. Appl. **11**, 044024 (2019). https://doi.org/10.1103/PhysRevApplied.11.044024
44. C. Liaskos, S. Nie, A. Tsioliaridou, A. Pitsillides, S. Ioannidis, I. Akyildiz, A new wireless communication paradigm through software-controlled metasurfaces. IEEE Commun. Mag. **56**(9), 162–169 (2018). https://doi.org/10.1109/MCOM.2018.1700659
45. L. Subrt, P. Pechac, Controlling propagation environments using intelligent walls. In: 2012 6th European Conference on Antennas and Propagation (EUCAP), pp. 1–5 (2012). https://doi.org/10.1109/EuCAP.2012.6206517

46. L. Subrt, P. Pechac, Intelligent walls as autonomous parts of smart indoor environments. IET Commun. **6**(8), 1004–1010 (2012). https://doi.org/10.1049/iet-com.2010.0544
47. DOCOMO, N.: Docomo conducts world's first successful trial of transparent dynamic metasurface. Technical report, NTT DOCOMO, INC. www.nttdocomo.co.jp/english/info/media_center/pr/2020/ 0117_00.html
48. W. Tang, X. Li, J.Y. Dai, S. Jin, Y. Zeng, Q. Cheng, T.J. Cui, Wireless communications with programmable metasurface: transceiver design and experimental results. China Commun. **16**(5), 46–61 (2019)
49. 5G: Study on channel model for frequencies from 0.5 to 100 GHz, ETSI TR 138 901 v14.3.0. Technical report, ETSI (2018)